The Flux and the Charge Ratio of Atmospheric Muons and Neutrinos

I. M. Brancus

Institute of Nuclear Physics and Nuclear Energy – Horia Hulubei, Bucharest, Romania

Abstract. The flux and the muon charge ratio, the ratio of positive to negative atmospheric muons, carry information which controls calculations of the neutrino fluxes and the hadronic interactions of the parent particles. WILLI is a rotatable stack of scintillators detectors, which allows measurements of the charge ratio of low energy atmospheric muons, incident under different zenith and azimuth angles by observing the lifetime of the stopped positive and negative muons. The measured data of the energy and the angle dependence of the muon charge ratio (which displays a pronounced East-West effect due to the influence of the geomagnetic field) control advanced Monte Carlo simulations of the flux of atmospheric muons and neutrinos. Results of extensive CORSIKA simulations taking explicitly into account the solar modulation of the flux of primary cosmic rays, the geomagnetic field and its cut off, are compared with recent measurements of atmospheric muon flux and charge ratio for various sites of different geomagnetic coordinates.

1 Introduction

Atmospheric muons arise from the decay of pions and kaons, generated in high-energy collisions of primary cosmic rays with nuclei of the Earth atmosphere, a phenomenon called Extensive Air Shower (EAS). Muons are unstable and decay to electrons or positrons and neutrinos with a half-life $\tau_\nu = 2.2$ μs. Muons interact weakly with matter and show reduced electromagnetic interactions, they pass relatively undisturbed through the atmosphere before being stopped by interactions with the material of the Earth. Their flux is influenced by the geomagnetic field.

This paper presents the results of flux and charge ratio calculations of atmospheric muons for different locations, comparing the outcome of extensive Monte Carlo simulations, using the CORSIKA simulation program [1], with values from semi-analytical approaches and with experimental data measured with the electromagnetic calorimeter (WILLI). The neutrino fluxes, simulated with CORSIKA are compared with other calculations and the influence of hadronic interaction models is investigated.

2 The Relevance of the Muon Flux of Cosmic Ray Muons for the Atmospheric Neutrino Anomaly and Cosmogenic Radio-Nuclide Production

The cosmic rays muons originate from decay of hadronic secondaries produced in particle cascades ("air showers") by primary cosmic rays:

$$\pi^{\pm} \rightarrow \mu^{\pm} \div \nu_{\mu}(\tilde{\nu_{\mu}}) \quad 100.0\% \quad \text{lifetime} \quad 2.6 \cdot 10^{-2}\mu s$$
$$K^{\pm} \rightarrow \mu^{\pm} \div \nu_{\mu}(\tilde{\nu_{\mu}}) \quad 63.5\% \quad \text{lifetime} \quad 1.2 \cdot 10^{-2}\mu s$$
$$\mu^{+} \rightarrow e^{+} + \nu_{e} + \tilde{\nu_{\mu}}$$
$$\mu^{-} \rightarrow e^{-} + \tilde{\nu_{e}} + \nu_{\mu}$$

It is immediately obvious that the muon flux is strongly related to the neutrino flux and that the ratio of positive to negative atmospheric muons, the muon charge ratio, $R_{\mu}(\mu^+/\mu^-) \sim R(\nu_e/\tilde{\nu_e})$ maps the ratio of neutrino and antineutrinos, providing relevant information for neutrino anomaly [2, 3].

Super-Kamiokande [4] and other experiments showed that the ratio of miuonic to electronic neutrinos is much smaller than the theoretical prediction, $(R(\mu/e)_{\text{observed}}/R(\mu/e)_{\text{predicted}} \ll 1$, phenomenon known as the neutrino anomaly. This observation is interpreted in terms of neutrino flavour oscillations. In addition, the flux and the muon charge ratio carry information on the current formulations of hadronic interaction models, adopted for the calculations of the fluxes.

The knowledge of the atmospheric muon flux is also of interest for geophysical applications [5]. Thus the muogenic production of the radioactive nuclide ^{36}Cl, $(T_{1/2} = 3 \times 10^7$ years), e.g. by α-removal from ^{40}Ca or via reactions of secondary neutrons from muon induced spallation is an important background, to be taken into account, when dating geomorphic surfaces. It has been shown that at depth below few meters, ^{36}Cl production in calcite is initiated most entirely by cosmic ray muons. A spectacular and illustrative example had been the estimate of the neutron flash of the Hiroshima bomb by determining ^{36}Cl in the tomb stones of Hiroshima [6].

3 Simulation of Extensive Air Showers with CORSIKA Including Geomagnetic Influences

The simulation program CORSIKA [1] describes the development of extensive air showers with primary energy larger than 10^{14} eV [2]. A special feature of CORSIKA program is the optional use of alternatively six different models for the description of the high energy hadronic interaction: DPMJET II.5 [7], QGSJET [8], VENUS [9], SIBYLL [10] and three different models for the description of low energy hadronic interaction: GHEISHA [11], UrQMD 1.1 [12] and DPMJET, which includes some extensions lowing the simulation of hadronic interaction down to 1 GeV. The threshold between the high and low energy models is set by default to $E_{lab} = 80$ GeV/n.

The calculation of the geomagnetic cutoff is done in a Monte Carlo procedure of the possible particle trajectories in the so called back-tracking method. Instead of tracking primary protons from outer space to the Earth's surface, antiprotons from the surface are retraced to the outer space. That enables the calculation of a table of allowed and forbidden trajectories. The input in the table depends on the location on the Earth, the arrival direction and the particle momentum [13].

The particle tracking starts at 112.83 km, the top of the atmosphere as defined in CORSIKA. The particle tracking is based on GEANT 3.21 [14]. The influence of the local magnetic field in the atmosphere is included in CORSIKA through the approximation of homogeneous field, as described by the International Geomagnetic Reference Field for the year 2000 [15]. The extended CORSIKA code accounts for the seasonal variations of different regions by seven atmospheric models [13].

The simulations have been done with the standard CORSIKA version 6.014 using the planar atmospheric model, for zenith angles $\theta < 30°$, and with the curved CORSIKA version, for the simulations of the East-West effect of the atmospheric muons and for all simulations of the atmospheric neutrinos.

The different primary particles, proton and helium, have been simulated in a ratio following the absolute fluxes reported by the AMS prototype mission [17]. The absolute fluxes of heavier nuclei have been taken from a compilation of Wiebel-Sooth *et al.* [18] . There are various experiments, reported in literature, about experimental results of the atmospheric flux and the muon charge ratio: BESS [19], CAPRICE [20], OKAYAMA telescope [21]. Figure 1 compares data with the present CORSIKA simulations [13].

The calculation with DPMJET as well as the calculations with VENUS + UrQMD generally agree well with the experimental data. Only the GHEISHA results show a strange enhancement of the differential muon flux for low energies and a quite different momentum dependence.

3.1 Semi-Analytical Approximations of the Atmospheric Muon Flux

In view of detailing geomagnetic effects, the muon fluxes have been calculated [20] for two different locations with different magnetic cutoff: Hiroshima (34°N, 132°E) with the geomagnetic cutoff 11.6 GV and Bucharest (44°N, 26°E) with geomagnetic cutoff of 5.6 GV. There are various semi-analytical approximations on the market. The validity of the formula given by Gaisser [23] is restricted to muon energies $E > 10$ GeV. The formulation of Judge and Nash [24] tuned to experimental results, may be useful for the consideration of low energy muon flux. But it invokes various ad hoc parameters. Figure 2 compares the results of muon flux simulated with CORSIKA for Bucharest and Hiroshima with results from semi-analytical formulae of Gaisser and Judge and Nash, respectively and with experimental data from BESS. As expected, it displays disagreement, in particular with Gaisser formula, at low energy.
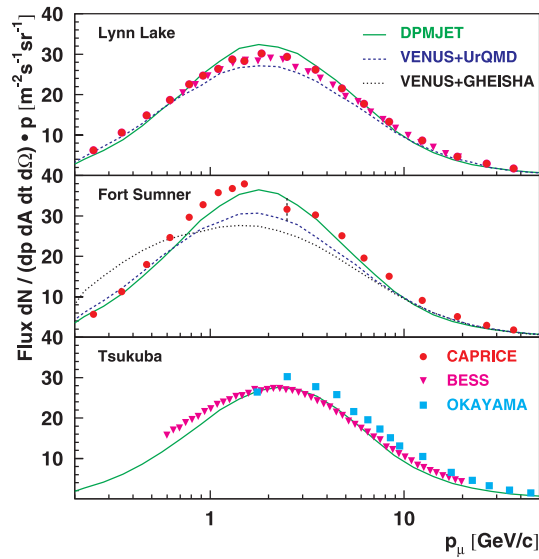
Figure 1. The differential flux of vertical muons simulated on basis of different hadronic interaction models and compared with experimental results. Note: the flux is multiplied by the muon momentum p.
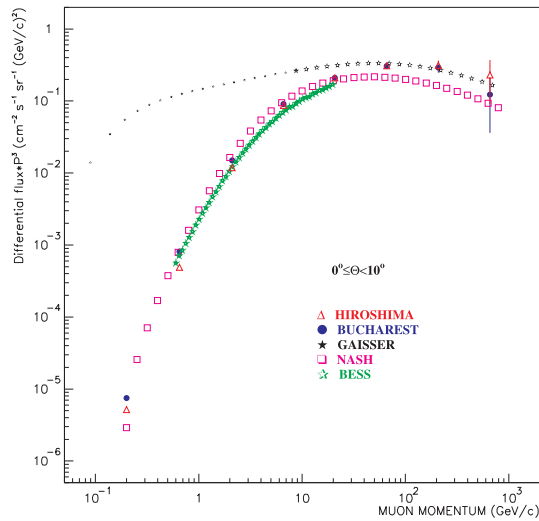

Figure 2. The vertical muon flux predicted by CORSIKA compared with results of the BESS experiment and semi-analytical formulae.

4 Muon Charge Ratio Measurements

4.1 Muon Charge Ratio Data

The charge ratio $R_\mu(\mu^+/\mu^-)$ of atmospheric muons provides a sensitive test of the simulation of the fluxes as the primary and secondary component of cosmic rays
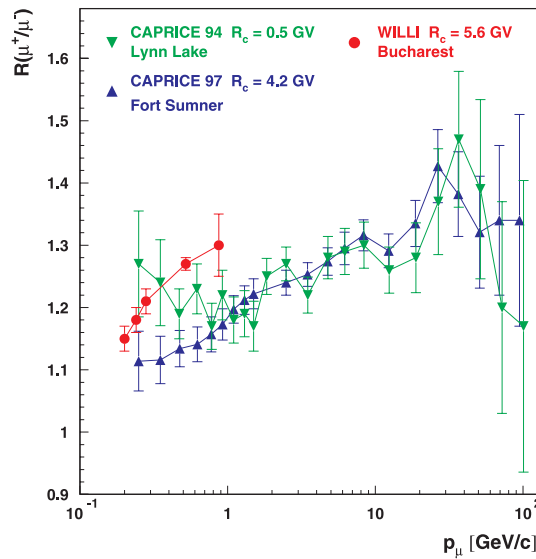
Figure 3. Compilation of muon charge ratio results.

is influenced by the geomagnetic field. This influence leads to the latitude effects of the flux and to the East West effect, due to the fact that in the east and west plane the muons of positive and negative charge have different path lengths from the production level, and consequently the decay probability for low-energy muons is modified. Figure 3 displays muon charge ratio data indicating large differences for muons with low incident energy.

4.2 WILLI Detector

The WILLI detector determines the muon charge ratio by measuring the life time of stopped muons in the detector layers, which is different for positive and negative muons: stopped *positive* muons decay with a lifetime of 2.2 μs, while *negative* muons are captured in the atomic orbits, leading to an effectively smaller lifetime depending on the stopping material. The uncertainties in the detector efficiency and the geometry are the same for positive and negative muons. Figure 4 presents the initial configuration for measurements of the charge ratio of vertically incident muons [25] and the later extension of the device WILLI [26] for adjusting the zenith and azimuth direction of muon incidence.

A good event is a stopped and decaying muon triggering the telescope, but not penetrating to the bottom of the scintillator stack, together with the appearance of a delayed particle, which disappears in the surrounding of the stopping locus. From the time interval of incoming and decaying particle the spectrum of the decay times is registered.
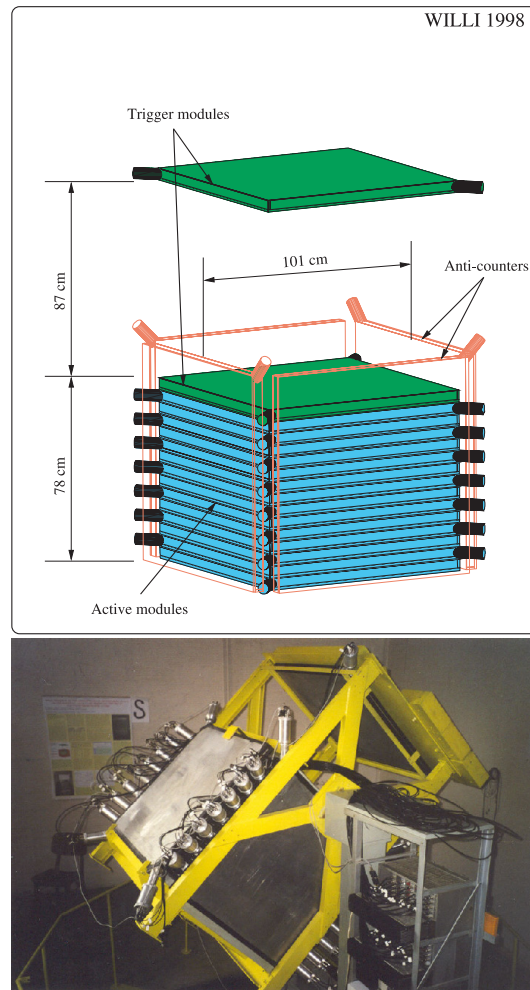
Figure **4.** The vertical and the rotatable WILLI detector.

The total decay curve of all muons measured in the detector is a superposition of several decay laws, containing 3 detector dependent constants, which have been determined by extensive detector simulations using the code GEANT. The muon charge ratio is obtained by fitting the decay measured spectrum with the simulated curve. The decay curve of the muons has the expression:

$$\frac{dN}{dt} = \left[\frac{N_0}{(R+1)}\right]\left[R\frac{c_0}{\tau_0}\exp\left(-\frac{t}{\tau_0}\right) + \sum\frac{c_j}{\tau_j}\exp\left(-\frac{t}{\tau_j}\right)\right]$$

where, $R(\mu^+/\mu^-) = N^+/N^-$ represents the muon charge ratio, N^+, N^- is the number of pozitive and negative muons, respectively, τ_j indicates the lifetime of
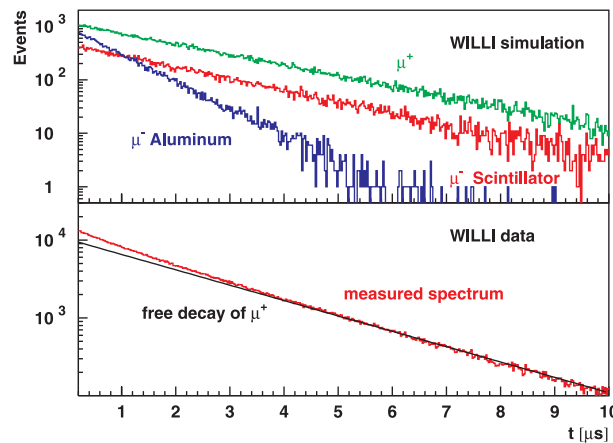
Figure **5.** The muon decay curves, simulation and data.

μ^- with the index j describing the absorber and the index 0 standing for positive muons.

Figure 5 displays the results of simulations exhibiting the exponential decay for different materials and the comparison of the experimental decay curve with the free decay of positive muons.

4.3 Results

Figure 6 compares the muon charge ratio data for vertical muons and for data measured separately in East and West direction for muons with WILLI detector inclined at $45°$, displaying a pronounced East-West effect in the energy range < 1 GeV [26]. Following the simulations, the anisotropy could be attributed to the anisotropy of primary proton flux caused by the geomagnetic cut-off, because the local field strengths in Bucharest is week.

An Est-West effect on the atmospheric muon flux was also observed in the Okayama experiment [27].

In Figure 7 the CORSIKA results for the muon charge ratio are compared with experimental data from different experiments [13]. The results obtained with the GHEISHA model are far from the experimental observations. but there are also discrepancies between the results of DPMJET and VENUS + UrQMD, the later results underestimating the experimental data (especially at lower and intermediate muon energies). The DPMJET results agree generally well with the data, except of the CAPRICE results of Fort Sumner. The influence of the geomagnetic cut-off on the muon charge ratio can be seen by comparing the CAPRICE and BESS results for Lynn Lake, the WILLI results from Bucharest and the BESS results from Tsukuba. At higher energy the ratio stays nearly constant, but it decreases when the geomagnetic cut-off clips the great excess of low energy protons, as can be observed in the results from Bucharest and Tsukuba. This effect is well reproduced
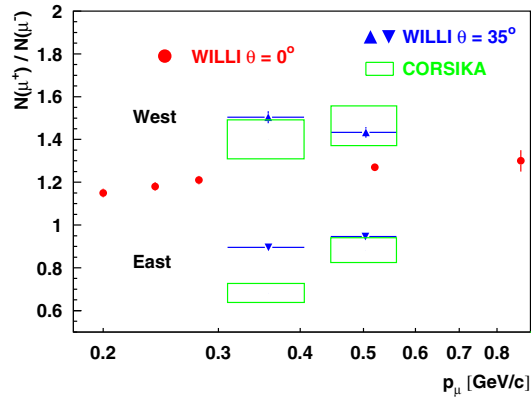
Figure **6.** The energy dependence of the muon charge ratio; comparison of experimental data with CORSIKA simulations values.

by CORSIKA using DPMJET as interaction models. The CAPRICE results at Fort Summer are doubtful, displaying almost the same dependence on the momentum as the BESS results, though the geomagnetic cut-off is nearly three times higher.

The results obtained with the GHEISHA model are far from the experimental observations. but there are also discrepancies between the results of DPMJET and VENUS + UrQMD, the later results underestimating the experimental data (especially at lower and intermediate muon energies). The DPMJET results agree generally well with the data, except of the CAPRICE results of Fort Sumner. The influence of the geomagnetic cut-off on the muon charge ratio can be seen by comparing the CAPRICE and BESS results for Lynn Lake, the WILLI results from Bucharest and the BESS results from Tsukuba. At higher energy the ratio stays nearly constant, but it decreases when the geomagnetic cut-off clips the great excess of low energy protons, as can be observed in the results from Bucharest and Tsukuba. This effect is well reproduced by CORSIKA using DPMJET as interaction models. The CAPRICE results at Fort Sumner are doubtful, displaying almost the same dependence on the momentum as the BESS results, though the geomagnetic cut-off is nearly three times higher.

4.4 Calculation of the Atmospheric Neutrino Fluxes for KAMIOKA

The simulations of atmospheric neutrino fluxes are split in two separate calculations, [13]:

– the downward going neutrinos are simulated locally for Kamioka,
– while the upward going neutrinos are calculated for primary particles distributed over the entire Earth and only neutrino passing in a circle of 1000 km distance from Kamioka are used in further analysis.
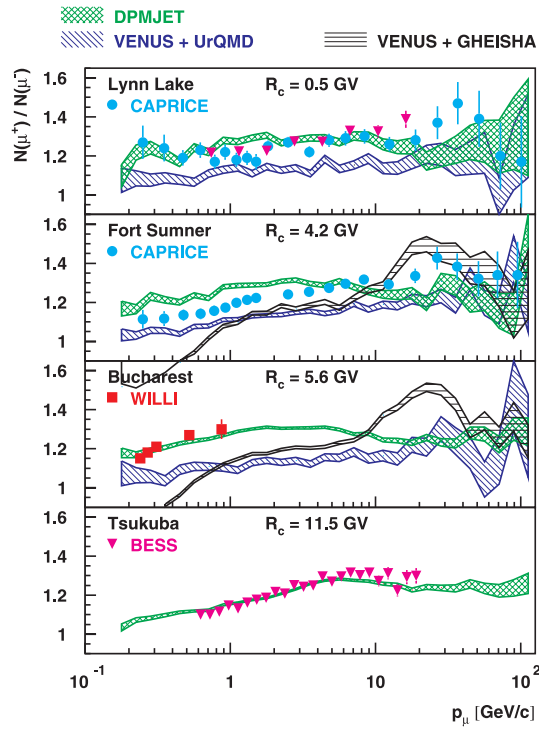
Figure **7.** The charge ratio of atmospheric muons calculated by CORSIKA on basis of different hadronic interaction models as compared to various experimental results.

Figure 8 shows results of CORSIKA using DPMJET II.5 as hadronic interaction models, compared with the calculations of Barr, Gaisser and Stanev (BGS) [28], Honda *et al.* (HKHM) [29] and Battistoni *et al.* (BFLMSR) [30].

The inclusive neutrino flux obtained with CORSIKA is lower than the fluxes given by BGS and HKHM, around 40% smaller, for energies < 1 GeV and comparable in GeV range. The agreement of BFLMSR with CORSIKA results using DPMJET turn out to be improved.

5 Concluding Remarks

– The knowledge of the *atmospheric muon flux* plays an important role in various studies of basic and applied physics research of interdisciplinary character.
– The measurement made using WILLI, inclined at $45°$, show a pronounced East-West effect, in good agreement with simulations data [13, 26] and with the East-West effect found in neutrino experiments [4].
– Using Monte Carlo simulations of atmospheric muon fluxes with CORSIKA [13] it was possible to test semi-empirical parametrizations of the muon flux [22].
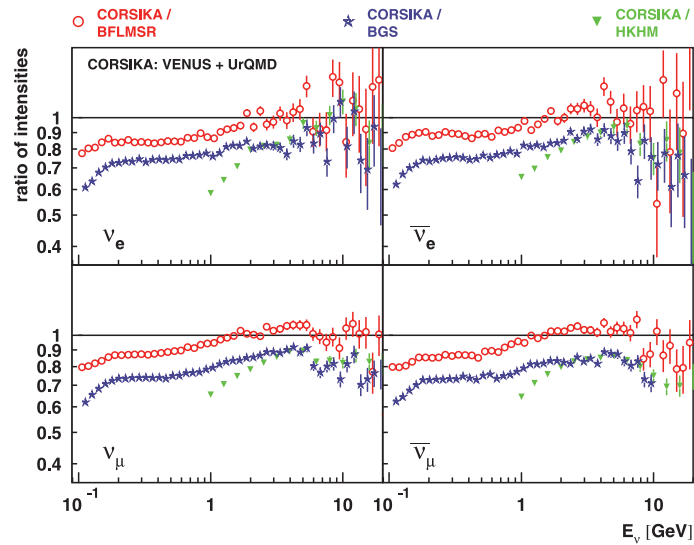
Figure **8.** The vertical differential intensities of the different neutrino flavours in Kamioka, displayed as a aratio between CORSIKA results, using DPMJET as hadronic interaction model, and the calculations of BGC [28], HKHM [29], BFLMSR [30].

– The hadronic interaction models used for muon and neutrino fluxes simulations are sensitively controlled by measurements of the muon charge ratio. In addition its experimentally observed azimuth variations demonstrate the influence of the geomagnetic field at muon energies < 1 GeV.

Acknowledgements

References

1. D. Heck *et al.*, *FZKA Report 6019* (1998).
2. J. Wentz *et al.*, *J. Phys. G. Nucl. Part. Phys* **27**, 1699 (2001).
3. R. Lipari, *Astropart. Phys.* **16**, 295 (2002).
4. Y. Fukuda *et al.*, *Phys. Lett. B* **433**, 9 (1988); *Phys. Lett* **81**, 1562 (1988).
5. J.O.H.Stone *et al.*, *Geochimica et Cosmochimica Acta* **62**, 433 (1988).
6. Annual report Beschleunigerlaboratorium der Universitat Munchen, 20 (2000).
7. J. Ranft, *Phys.Rev.D* **51**, 64 (1995).
8. N.N. Kalmykov *et al.*, *Nucl. Phys. B (Proc.Suppl)* **52B**, 17 (1997).
9. K. Werner, *Phys.Rev* **232**, 82 (1993).
10. J. Engel *et al.*, *Phys. Rev. D* **51**, 3525 (1992).

11. H. Fesefeldt, *RWTH Aachen Report No.PITHA-85/02*, 064313 (1985).
12. S.A. Bass *et al.*, *Progr. Part. Nucl. Phys* **41**, 255 (1998).
13. J. Wentz *et al.*, *Phys. Rev. D* **67**, 073020 (2003).
14. GEANT Detector Description and Simulation Tool, *CERN Program Library Long Write-Up W5013* (1993).
15. R.A. Langel *et al.*, *EOS Trans. Am. Geophys. Union* **7**, 182 (1992).
16. F.X. Kneizys *et al.*, *"MODTRAN 2/3 Report and LOWTRAN 7 Model"* Philips Lab., Hanscom AFB, MA. **83**, 59 (1996).
17. J. Alcaraz *et al.*, *Phys. Lett B* **490**, 27 (2000).
18. B. Wiebel-Sooth *et al.*, *Astron. Astropart* **330**, 389 (1989).
19. M. Motoki *et al.*, *Astropart. Phys* **19**, 113 (2003).
20. J. Kramer *et al.*, *Phys. Rev. Lett* **83**, 4241 (1999).
21. S. Tsuji *et al.*, *J. Phys. G* **27**, 1805 (1998).
22. B. Mitrica *et al.*, *FZKA Interner Bericht* KASCADE-Grande (2004).
23. T. Gaisser, *Astropart. Phys.* **16**, 285 (2002).
24. R.J.R. Judge and W.F. Nash, *Il Nuovo Cim. XXXV* **4**, 999 (1965).
25. B. Vulpescu *et al.*, *Nucl. Phys. Meth. Res. A* **414**, 205 (1998); *J. Ohys. G. Nucl. Part. Phys.* **27**, 977 (2001).
26. I.M. Brancus *et al.*, *Nucl. Phys A* **271**, 1044c (2003).
27. M. Tokiwa *et al. Proc. ICRC 2003* vol. 3, p.1171, Tsukuba, Japan.
28. G. Barr, T. Gaisser, T. Stanev, *Phys. Rev. D* **39**, 3532 (1989).
29. M. Honda *et al.*, *Phys. Rev. D* **52**, 4985 (1995).
30. G. Battistoni *et al.*, *Astropart. Phys.* **15**, 315 (2000).